

Published in final edited form as:

J Med Chem. 2009 January 22; 52(2): 445–455. doi:10.1021/jm8012213.

Comparative Positron-Emission Tomography (PET) Imaging and Phototherapeutic Potential of ¹²⁴I- Labeled Methyl- 3-(1'-iodobenzoyloxyethyl) pyropheophorbide-a vs. the Corresponding Glucose- and Galactose-Conjugates

Suresh K. Pandey¹, Munawwar Sajjad^{3,*}, Yihui Chen¹, Xiang Zheng¹, Rutao Yao³, Joseph R. Missert¹, Carrie Batt¹, Hani A. Nabi³, Allan R. Oseroff², and Ravindra K. Pandey^{1,*}

¹ PDT Center, Roswell Park Cancer Institute, Buffalo, NY 14263

² Department of Dermatology, Roswell Park Cancer Institute, Buffalo, NY 14263

³ Department of Nuclear Medicine, State University of New York, Buffalo, NY 14214

Abstract

In our present study, 3-(1'-*m*-iodobenzoyloxyethyl) pyropheophorbide-*a* methyl ester **1**, 3-(1'-*m*-iodobenzoyloxyethyl)-17²-{(2-deoxy)glucose} pyropheophorbide-*a* **2**, and 3-(1'-*m*-iodobenzoyloxyethyl)-17²-{(1-deoxy)galactose} pyropheophorbide-*a* **3** were synthesized and converted into the corresponding ¹²⁴I- labeled analogs by reacting the intermediate trimethyltin analogs with Na¹²⁴I. Photosensitizers **1–3** were evaluated for the PDT efficacy in C3H mice bearing RIF tumors at variable doses and showed a significant long-term tumor cure. Among the compounds investigated, the non-carbohydrate analog **1** was most effective. These results were in contrast to the *in vitro* data, where compared to the parent analog the corresponding galactose- and glucose derivatives showed enhanced cell kill. Among the corresponding ¹²⁴I-labeled analogs, excellent tumor images were obtained from compound **1** both tumor models (RIF and Colon-26) and the best tumor contrast was observed at 72 h post injection. Conjugating a glucose moiety to photosensitizer **1** diminished its tumor uptake, whereas with time the corresponding galactose analog showed improved tumor contrast.

Introduction

Molecular imaging is a newly emerging field in which the modern tools of molecular and cell biology are being combined together to the state-of-art technology for noninvasive imaging. The goals of this field are to develop technologies for studying biological processes as well as detect and monitor various diseases including cancer. Molecular imaging has its roots in nuclear medicine and in many ways is a direct extension of this existing discipline¹. In recent years, positron-emission tomography (PET), a noninvasive imaging technique that exploits the unique decay physics of positron-emitting isotopes has created enormous interest in tumor imaging in order to provide a functional or metabolic assessment of normal tissues or disease

*Address for correspondence ¹Ravindra K. Pandey, Ph.D., Professor and Distinguished Member PDT Center, Cell Stress Biology, Roswell Park Cancer Institute, Buffalo, NY 14263, Phone: 716-845-3203; Fax: 716-845-8920, E-mail: E-mail: ravindra.pandey@roswellpark.org. ³Munawwar Sajjad, Ph.D., Associate Professor, Department of Nuclear Medicine, State University of New York, Buffalo, NY 14214, Phone: 716-838-5889 ext. 118; Fax: 716-838-4918, E-mail: E-mail: msajjad@buffalo.edu.

Supporting Information Available: ¹H NMR spectra for compounds **1**, **2**, **3**, **6**, **9**, **10**, **12** and the analytical details of compounds **1–12**. This material is available free of charge via the Internet at <http://pubs.acs.org>.

conditions^{2,3}. PET with ¹⁸F-FDG is approved by the Center for Medicare and Medicaid Services for diagnosing, staging, and restaging lung cancer, colorectal cancer, lymphoma, melanoma, head and neck cancer, and esophageal cancer. Although ¹⁸F-FDG is an exquisite tumor-localizing tracer, it is not tumor-specific. The uptake of ¹⁸F-FDG reflects glucose use in essentially any tissue; its increased uptake in tumors is a result of increased and inefficient use of glucose. Other benign processes associated with cells that have increased glucose use, such as inflammatory cells or hyperplastic bone marrow or thymic cells, also have enhanced ¹⁸F-FDG uptake. Thus, increased ¹⁸F-FDG uptake is usually observed in infectious and inflammatory processes, inflammatory changes after surgery or irradiation and thymic or bone marrow hyperplasia after treatment. Additionally, the short half-life of ¹⁸F-isotope (110 min) limits its use in studies involving antibodies, and in photodynamic therapy (PDT), where the photosensitizers often take a considerably longer time to both accumulate in tumors as well as clear from the non-targeted organs⁴. In this respect, ¹²⁴I- is a better choice due to its half-life of 4.2 days and because it enables longitudinal imaging studies using animal PET. The labeling technique for ¹²⁴I-isotope is now well established and this approach is continuously being used in labeling a variety of biologically active molecules⁵.

For quite some time our laboratory has been investigating the utility of porphyrin-based compounds for the use in photodynamic therapy (PDT), which is now a well-established non-invasive modality for tumor treatment.⁶ A purified form of the hematoporphyrin derivative, developed in our Institute by Dougherty and coworkers has been approved worldwide for the treatment of various cancers and is being marketed by Axcan Pharmaceuticals, Canada⁷. One of the drawbacks of the hematoporphyrin derivative has been its skin phototoxicity; the patients are advised to be away from direct sunlight for 6–8 weeks after the treatment. Therefore, efforts are underway in various laboratories to develop a photosensitizer at least as effective as the purified form of the hematoporphyrin derivative but with reduced skin phototoxicity. At the PDT Center of our Institute, HPPH, a compound derived from chlorophyll-a has shown promising results with limited skin phototoxicity and it is currently in Phase I/II clinical trials⁸. Efforts are currently underway in our and other laboratories to develop target-specific agents by conjugating the porphyrin-based compounds to target-specific moieties for binding to those proteins known for their over-expression in tumor cells⁹.

For optimizing the PDT treatment by a “see and treat approach”, we have been exploring the utility of tumor-avid photosensitizers as vehicles to deliver the desired imaging moiety to tumors. We have previously reported the advantages of this approach in developing certain HPPH-cyanine dye and HPPH-DTPA conjugates for PDT/fluorescence imaging and PDT/MR imaging respectively¹⁰. However, fluorescence imaging (planer imaging) has limited applications for imaging deeply-seated tumors due to the relatively low tissue penetration ability of the visible light¹⁰, whereas the MR imaging suffers from low sensitivity at the molecular target level. In contrast, nuclear imaging, e. g., PET and Single Photon Emission Computer Tomography (SPECT), has been widely used for human tomographic imaging as a result of using high energy photons and is intrinsically suited for molecular imaging. Therefore, we have been interested in using certain tumor-avid porphyrin-based molecules as vehicles to deliver the desired nuclide to the target-site for nuclear imaging¹¹. In our earlier study, as a proof of principle approach, we introduced ¹²⁴I nuclide in methyl pyropheophorbide-a and this compound showed its potential in both tumor imaging and phototherapy in mice (C3H) bearing RIF tumors¹².

It has been reported by various investigators that introduction of glucose- and β -galactose moieties in photosensitizers¹³ leads to increased efficiency in tumor uptake. It is believed that ¹⁸F-FDG, an analog of glucose, enters cells *via* glucose transporters (GLUT). Speizer explored the utility of glucose by incorporating it to a fluorescent molecule into human erythrocytes and this approach was then extended in developing other analogs¹⁴. In a similar

approach, recently, a pyropheophorbide-2-deoxyglucosamide has been reported as a new photosensitizer targeting the glucose transporters¹⁵, and it is proposed to be trapped in tumor cells via the GLUT/hexokinase pathway.

To investigate the utility of the carbohydrate moieties in developing target-specific photosensitizers, we conjugated a highly effective photosensitizer (HPPH, a chlorophyll derivative) with a series of carbohydrates and among all the compounds, the HPPH- β -galactose conjugate produced higher photosensitizing efficacy than HPPH in mice bearing RIF tumors¹⁶. Based on these findings, we hypothesized that compared to compound **1**, the corresponding glucose- **2** and galactose **3** analogs (Figure 1) should produce improved PET imaging and PDT efficacy. The comparative *in vivo* imaging, biodistribution and therapeutic potential of these compounds were investigated in BALB/c mice bearing Colo-26 tumors.

Results and Discussions Chemistry/Radiochemistry

In a sequence of reactions, compound **1** was synthesized from methyl pheophorbide-a¹⁷, which in turn was isolated from *Spirulina pacifica* by following the methodology developed by Smith *et al*¹⁸. The methyl ester functionality present at position-17² was then hydrolyzed with aqueous LiOH in an inert atmosphere to yield the corresponding carboxylic acid **4**. The activated succinimido derivative **5** was reacted with 2-amino-2-deoxyglucose and the compound **2** was obtained in 56% overall yield. By following a similar approach, compound **4** was also condensed with 1-amino-1-deoxy-galactose tetraacetate in presence of (Benzotriazol-1-yloxy)tripyrrolidinophosphonium hexafluorophosphate (PyBOP) to produce intermediate **6**, which upon standard acetyl deprotection by treating with sodium methoxide afforded the corresponding galactose conjugate **3** in 48% yield (Scheme 1).

For labeling the glucose- **2** and the galactose-**3** conjugates radiospecifically with Iodine-124, trimethylstannyl derivatives **9** and **11** were synthesized from **1** by following the reaction sequences illustrated in Scheme 1. In brief, compound **4**, obtained by aq. LiOH hydrolysis of **1**, upon reacting with hexamethylditin gave the corresponding trimethylstannyl analog **7**, which was converted to the corresponding succinimido derivative **8**. Further reaction of **8** with 2-amino-2-deoxyglucose produced the trimethylstannyl derivative **9** in 68% yield. For the preparation of **11**, the trimethylstannyl derivative **7**, was directly reacted with 1-amino-1-deoxygalactose tetraacetate in presence of PyBOP and gave the acetylated galactose conjugate **10** in 55% yield. The deprotection of the acetoxy groups on treatment with sodium methoxide afforded the desired galactose analog **11** in modest yield. All final compounds were analyzed by HPLC for chemical purity (retention times for the glucose (**2**)- and galactose (**3**)-conjugates were 8.17 min and 8.02 min respectively (for details, see the experimental section). Conjugation of 2-deoxyglucose and 1-deoxygalactose with the lead compound **1** at 17²-position produced the corresponding conjugates **2** and **3**, having identical molecular weight and lipophilicity, but with a significant difference in the HPLC retention times (see Supporting Information).

For ¹²⁴I-labeling, trimethylstannyl derivatives **9**, **11** and **12** were separately reacted for 15 minutes at room temperature with NaI¹²⁴ (produced in UB cyclotron facility¹⁹ in the presence of 1,3,4,6-tetrachloro-3 α ,6 α -diphenylglucuril. After 15 minutes the bead was removed and radioactive reaction mixture was purified by HPLC. The peaks corresponding to the desired iodinated products **1–3** were collected and the ¹²⁴I- labeling was confirmed by RadioTLC.

Comparative biodistribution of ^{124}I labeled pyropheophorbide-a (1), its glucose (2) and galactose (3) derivatives

Four C3H mice were implanted with RIF tumors over the right shoulder. With this tumor location, mice could be restrained in a Plexiglas holder and PDT could be performed without using any anesthesia procedure. Figure 2 shows the *in vivo* bio-distribution results, in terms of percent injected dose per unit weight (%ID/g), for the three compounds at 24, 48, 72 and 96 hours post-injection. Among the three compounds, compound **1** had the highest tumor uptake value at 24 and 48 hrs time points, topping at 4.1%ID/g at the 24hr post injection. Compound **3**, the galactose derivative of compound **1**, was found to have higher uptake values at the 72 and 96 hrs time points, however it also had considerably higher liver and spleen uptake at all time points. Compound **2**, the glucose analog of compound **1** had the least tumor uptake among all compounds at all time points, and it also had lower spleen and liver uptake than **3** but higher than that of **1**. The corresponding animal PET images showed clearly the tumor site with **1** at time points 24 hours after injection, indicating its high uptake; however the high uptakes of **2** and **3** in liver compared to that of **1** undermined the prominence of tumor accumulation for **2** and **3**. The %ID/g ratios of tumor and liver were 0.32, 0.08 and 0.05 for **1**, **2** and **3** respectively at 24h post injection. At 48h and 72h the tumor contrast became higher for **1** as it was cleared rapidly from spleen and liver (compared to tumor) resulting in an improved tumor image at 48h and 72h post injection. In case of both **2** and **3** there was no significant improvement was observed over time. The %ID/g ratio of tumor and liver was 0.56, 0.13 and 0.06 for **1**, **2** and **3** respectively at 48 hrs post injection.

The tumor volume in each study was obtained by first manually placing an elliptical cylinder that contains the tumor volumes and then count the voxels with intensity >25% of the maximum of the cylinder volume.

Comparative Biodistribution of ^{124}I -photosensitizer **1** in C3H (RIF tumors) and BALB/c mice (Colon 26 tumors)

Based on the results that the lead compound **1** had the best tumor specificity in mice with RIF tumors, we tested it in BALB/c mice bearing Colon-26 tumors by PET imaging and biodistribution studies. Four mice per time point were sacrificed for comparing the biodistribution of **1** in two tumor models. As can be seen in Figure 3, compound **1** (^{124}I -labeled) produced higher tumor accumulation in Colon-26 tumor than the RIF tumor at each time point. The calculated uptake value of compound **1** in Colon-26 tumor was 4.6%ID/g, 4.4%ID/g, 2.5%ID/g, and 2.0%ID/g while in RIF tumor it was 4.1%ID/g, 2.1%ID/g, 0.8%ID/g and 0.6%ID/g at 24, 48, 72 and 96h post injection respectively. Though compound **1** produced similar uptake at 24 h post injection in both Colon-26 and RIF tumors, the uptake value in Colo-26 was 2-fold higher at 48h and 3-fold higher at 72 h and 96 h post injection. These data suggest that the clearance rate of photosensitizer **1** from other organs and in RIF tumors is faster than in Colo26 tumors. Also, compound **1** showed slightly higher blood uptake in BALB/c mice than C3H mice. Interestingly, in other organs, compound **1** produced lower uptake in BALB/c mice than the C3H mice. The higher uptake of **1** in Colon-26 tumors compared to RIF tumors and its relatively lower organs' uptake in BALB/c mice may be responsible for enhanced tumor images.

The mice were imaged at 24, 48, 72 and 96 hrs post injection of ^{124}I -labeled **1** and as can be seen from Figure 4 the PET images of a BALB/c mouse bearing Colon-26 tumor, the tumor was progressively more visible over time as a result of elevated tumor uptake compared to other organs.

To quantify the visibility of tumor in the images, the tumor uptake in each study was measured in terms of a relative uptake value (*RUV*), which is defined as

$$RUV = \frac{\text{max_voxel_activity_in_tumor}(Bq/cc)}{\text{total_body_activity_in_image}(Bq)/\text{total_body_volume_in_image}(cc)}$$

The animal's body volume in the image was delineated by defining an iso-contour ROI with the ROI's lower threshold set at about 3–6% of the maximum voxel intensity of the dataset and manually adjusted according to visual inspection. Using *RUV* avoids the need to collect the activity excreted through physiological process (excrements) from the time of injection to scan acquisition, and reflects the tumor uptake within the interested body section in the same way as the more well known *SUV*. The *RUV* values for images obtained are shown in Figure 5. The *RUV* value for the ^{18}F -FDG study was 4.0, slightly higher than that of the ^{124}I -I tracer applied to RIF tumor, but lower than the colo-26 tumor with ^{124}I -I tracer at 48 hours post injection. The colo-26 tumor showed a higher *RUV* values than RIF tumor after 48 hours of injection of ^{124}I -I agent.

Figure 6 shows the relative activity in tumor as compared to the activity in the whole section of body imaged. The relative tumor activity value for the ^{18}F -FDG RIF tumor study was 0.035, similar to that of ^{124}I -I tracer in RIF tumor, which remained about constant for the three post-injection scans over 3 day period. The Colon-26 tumor, however, showed increasing relative quantity of activity in the tumor. This explains the increasing prominence of Colon-26 tumor in images over time.

Comparative *in vitro* uptake and PDT efficacy

The cell uptake of photosensitizer **1** and the corresponding galactose and glucose analogs **2** and **3** respectively were measured at 3 and 24 h post injection by fluorescence (see the experimental section). As can be seen from Figure 7, all three compounds with or without a carbohydrate moiety showed higher uptake at 24 h post-incubation.

The photosensitizing abilities of compound **1** and its glucose- **2** and the galactose- conjugate **3** were tested in radiation-induce fibrosarcoma (RIF) cells at variable concentrations (0.25, 0.5, 0.25, 1, 2 and 5 μM), various light doses (0, 1, 2, 4 J/cm^2) and two incubation time points (4 hrs and 24 hrs). A drug and light dose-dependent response was observed as determined by the MTT assay. From the results summarized in Figure 8 (only 24 h post incubation results are shown), it can be seen that both the carbohydrate conjugates **2** and **3** are more effective than the corresponding non-carbohydrate analog **1** at the given conditions.

In vivo PDT efficiency of pyropheophorbide-a **1** and its glucose-conjugate **2** and the galactose- conjugate **3**

For determining the *in vivo* PDT efficacy of the title compounds, the C3H mice (five mice/group) bearing RIF tumors (4–5 mm in diameter) were injected intravenously at variable drug doses (0.5, 1.0 and 1.5 $\mu\text{mol}/\text{kg}$). The tumor area was then irradiated with a 1 cm^2 laser light (665 nm, 135 J/cm^2 , 75 mW/cm^2 for 30 min) at 24 h post-injection. The tumor re-growth was observed daily and when the tumor size reached the threshold of 400 mm^3 , the mice were sacrificed. From the results summarized in Figure 9, it can be seen that at the lowest drug dose, (0.50 $\mu\text{mole}/\text{kg}$), one out of five mice was tumor free with the glucose-conjugate **2**, whereas the non-conjugate **1** and galactose-conjugate **3** did not show any tumor response, though between **1** and **3**, **3** showed improved tumor cure. Upon increasing the drug dose (1.00 $\mu\text{mole}/\text{kg}$), two out of five mice were tumor free for **2**, while one out of five mice was tumor free for compound **1**. For compound **3**, this dose was found to be toxic and all five mice died within

24h post PDT. When the dose was escalated to 1.5 $\mu\text{mol/kg}$, the cure rate for compound **1** showed a significant increase in photosensitizing ability and four out of five mice were tumor free at day 60. At the same drug dose and light treatment parameters some toxicity was observed for compound **2**, where two mice died within 24 h post PDT and two out of remaining three mice were tumor free by day 60. This drug dose was found to be too toxic for compound **3** and all five mice died within 24 h post light treatment. Further evaluation of these photosensitizers at variable drug and light doses in different tumor models is currently in progress.

Conclusion

PDT is a localized form of cancer treatment and has several advantages over other cancer treatment modalities. Most of the porphyrin-based compounds and those evaluated in our present study show optimal tumor uptake at >24 h. Therefore, for developing a single bifunctional agent for PET imaging and PDT, it is necessary to label the desired photosensitizer (s) with radionuclide having long half-life. With ^{124}I -labeled (half-life: 4.2 days) agent **1**, we were able to detect the tumors by PET imaging in two different models (RIF and Colon-26). The long residence time of the photosensitizer in tumor, as confirmed by the RUV and relative tumor activity values, also indicated great therapeutic potential. Compared to compound **1**, the corresponding glucose- **2** and galactose **3** analogs showed higher uptake in both Colon-26 and RIF cells. However, the *in vivo* biodistribution results obtained from the C3H mice bearing RIF tumors revealed that between the glucose- and galactose conjugates, the galactose conjugate **3** had higher tumor uptake. Interestingly, due to a high uptake of the carbohydrate derivatives in liver and spleen, the parent molecule **1** produced the best tumor contrast in both RIF and Colon-26 tumor models. Further studies to investigate the imaging potential of these and a series of PEG analogs with variable lipophilicity over ^{18}F -FDG in a series of tumor models are currently in progress.

Experimental Section

Chemistry

All chemicals were of reagent grade and used as such. Solvents were dried using standard methods. Reactions were carried out under nitrogen/argon atmosphere and were monitored by precoated (0.20mm) silica TLC plastic sheet (20 \times 20 cm) strips (POLYGRAM[®] SIL N-HR) and/or UV-visible spectroscopy. Silica gel 60 (70–230 mesh, Merck) was used for column chromatography. Melting points were determined on Fisher - Johns melting point apparatus. UV-visible spectra were recorded on a Varian (Cary 50 Bio) spectrophotometer. ^1H -NMR spectra were recorded on a Bruker AMX 400 MHz NMR spectrometer at 303 K. Proton chemical shifts (δ) are reported in parts per million (ppm) relative to CDCl_3 (7.26 ppm), pyridine- d_5 (7.22ppm, most downfield) or TMS (0.00 ppm). Coupling constants (J) are reported in Hertz (Hz) and s, d, t, q, p, m and br refer to singlet, doublet, triplet, quartet, pentet, multiplet and broad respectively. HRMS data were obtained from Mass Spectroscopy facility of Michigan State University. Analytical HPLC was used to assess the purity of compounds. A Waters (Milford, MA) system including Waters 600 Controller, Delta 600 pump and 996 Photodiode Array Detector was used. Reverse phase Symmetry[®] C18, 5 μm , 4.6 \times 150 mm column (Waters) was used under isocratic setting of MeOH/H₂O for final compounds (**1–3**, and their trimethyltin analogs). Solvent flow rate was kept constant at 1.00 mL/min and the detector was set at 254, 410, 535 & 660 nm. All final products were found to be >95 % pure and their retention time is reported in characterization section. Cold reactions were first carried out and the products were analyzed in the above HPLC system. However in case of final I-124 radiolabeling (hot reaction), HPLC data obtained from the above system were transferred to another system comprised of a Chrom Tech Iso-2000 pump, Hitachi L-4000 UV detector and a radiation detector. These detectors are connected to a computer with HP Chemstation

software via HP 35900E interface. A Bioscan system 200 imaging scanner was used for thin layer chromatography of the radiolabeled compounds.

Synthesis of 3-{1'-(*m*-iodobenzoyloxy)ethyl}pyropheophorbide-*a* methyl ester

(1)—It was prepared by following the reported procedure (12). Yield: 77%. Analytical RP HPLC (95/5: MeOH/H₂O; Symmetry): $t_R = 20.97$ min, >96%. UV-vis (CH₂Cl₂): 662 (4.75×10⁴), 536 (1.08×10⁴), 505 (1.18×10⁴), 410 (1.45×10⁵). ¹H-NMR (CDCl₃; 400 MHz): δ 9.76, 9.55 and 8.56 (all s, 1H, meso-H); 7.76 (s, 1H, ArH); 7.64 (d, J=6.8, 1H, ArH); 7.30 (d, J=8.0, 1H, ArH); 7.05 (t, J=8.2, 1H, ArH); 6.00 (q, J=6.9, 1H, 3¹-H); 5.28 (d, J=19.8, 1H, 13²-CH₂); 5.13 (d, J=19.8, 1H, 13²-CH₂); 4.70 (d, J=12.0, 1H, OCH₂Ar); 4.56 (dd, J=3.2, 11.6, 1H, OCH₂Ar); 4.48–4.53 (m, 1H, 18-H); 4.30–4.33 (m, 1H, 17-H); 3.72 (q, J=8.0, 2H, 8-CH₂CH₃); 3.69, 3.61, 3.38 and 3.21 (all s, all 3H, for 17²-CO₂CH₃ and 3× ring CH₃); 2.66–2.74, 2.52–2.61 and 2.23–2.37 (m, 4H, 17¹ and 17²-H); 2.18 (dd, J=2.8, 6.4, 3H, 3¹-CH₃); 1.83 (d, J=8.0, 3H, 18-CH₃); 1.72 (t, J=7.6, 3H, 8-CH₂CH₃); 0.41 (brs, 1H, NH); -1.71 (brs, 1H, NH). HRMS for C₄₁H₄₃N₄O₄I: 782.2329 (Calculated); 783.24 (Found, MH⁺). Anal. Calcd. For C₄₁H₄₃N₄O₄I: C, 62.91; H, 5.54; N, 7.16; I, 16.21. Found: C, 62.60; H, 5.59; N, 7.13; I 16.45.

Synthesis of 3-{1'-(*m*-trimethylstannylbenzyloxy)ethyl}pyropheophorbide-*a* methyl ester (12)

—It was synthesized following the reported procedure (12). Yield: 80%. Analytical RP HPLC (95/5: MeOH/H₂O): $t_R = 27.88$ min, >96%. UV-vis (CH₂Cl₂): 662 (4.75×10⁴), 605 (6.94×10³), 537 (7.77×10³), 506 (7.66×10³), 410 (9.58×10⁴). ¹H-NMR (CDCl₃; 400 MHz): δ 9.76, 9.54 and 8.55 (all s, 1H, meso-H); 7.43 (m, 2H, ArH); 7.36 (m, 2H, ArH); 6.01 (q, J=6.7, 1H, 3¹-H); 5.27 (d, J=19.1, 1H, 13²-CH₂); 5.12 (d, J=19.1, 1H, 13²-CH₂); 4.78 (dd, J=5.4, 11.9, 1H, OCH₂Ar); 4.61 (dd, J=1.7, 12.0, 1H, OCH₂Ar); 4.50 (q, J=7.4, 1H, 18-H); 4.32 (d, J=8.8, 1H, 17-H); 3.72 (q, J=7.8, 2H, 8-CH₂CH₃); 3.69, 3.61, 3.37 and 3.18 (all s, all 3H, for 17²-CO₂CH₃ and 3× ring CH₃); 2.66–2.75, 2.52–2.61 and 2.23–2.37 (m, 4H, 17¹ and 17²-H); 2.16 (m, 3H, 3¹-CH₃); 1.83 (d, J=7.2, 3H, 18-CH₃); 1.72 (t, J=7.6, 3H, 8-CH₂CH₃); 0.45 (brs, 1H, NH); 0.19 (s, 9H, Sn(CH₃)₃); -0.59 (brs, 1H, NH). Mass: Calculated for C₄₅H₅₂N₄O₄Sn: 831. Found: 854 (M⁺ + Na). Anal. Calcd. For C₄₅H₅₂N₄O₄Sn: C, 64.99; H, 6.30; N, 6.74. Found: C, 64.56; H, 6.66; N, 6.59.

Synthesis of 3-{1'-(*m*-iodobenzoyloxy)ethyl}pyropheophorbide-*a* (4)

—Aqueous LiOH (400 mg in 12 ml H₂O, purged with argon) was added to a solution of 3-{1'-(3-iodobenzoyloxy)ethyl}pyropheophorbide-*a* methyl ester (**1**) (200 mg, 0.25 mmol) in dry THF: MeOH (25: 8 ml) and the reaction mixture was stirred under argon at RT for 2 hr. The reaction mixture was neutralized with 2% AcOH in H₂O and compound was extracted with CH₂Cl₂ (100 ml). The organic layer was washed with H₂O (2×100 ml), dried over Na₂SO₄, concentrated and precipitated with hexanes to yield 185 mg (95%) crude product **6**, which was found to be pure enough for further use. UV-vis (MeOH/CH₂Cl₂): 663 (4.75×10⁴), 605 (6.81×10³), 539 (6.81×10³), 506 (6.61×10³), 411 (9.52×10⁴). ¹H-NMR (CDCl₃; 400 MHz): δ 9.72, 9.44 and 8.53 (all s, 1H, meso-H); 7.74 (s, 1H, ArH); 7.61 (d, J=8.0, 1H, ArH); 7.28 (m, 1H, ArH); 7.03 (m, 1H, ArH); 5.95 (q, J=6.8, 1H, 3¹-H); 5.25 (d, J=20.0, 1H, 13²-CH₂); 5.10 (d, J=20.0, 1H, 13²-CH₂); 4.65 (dd, J=4.0, 12.0, 1H, OCH₂Ar); 4.50 (m, 2H, OCH₂Ar & 18-H); 4.28 (d, J=7.6, 1H, 17-H); 3.67 (q, J=7.6, 2H, 8-CH₂CH₃); 3.58, 3.34 and 3.18 (all s, all 3H, for 3× ring CH₃); 2.55–2.72 and 2.20–2.35 (m, 4H, 17¹ and 17²-H); 2.15 (m, 3H, 3¹-CH₃); 1.78 (d, J=7.6, 3H, 18-CH₃); 1.68 (t, J=7.2, 3H, 8-CH₂CH₃); 0.02 (brs, 1H, NH); -1.70 (brs, 1H, NH). HRMS for C₄₀H₄₁N₄O₄I: 768.2174 (Calculated); 769.2207 (Found, MH⁺).

Synthesis of 3-{1'-(*m*-iodobenzoyloxy)ethyl}pyropheophorbide-*a* succinimidyl ester (5)

—Compound **4** (100 mg, 0.13 mmol) was activated with DCC (40 mg, 0.20 mmol) and N-hydroxysuccinimide (25 mg, 0.22 mmol) in DMF (3 mL). After stirring at RT overnight,

DCU was filtered off and the filtrate was concentrated and chromatographed over a silica column with 2.5% MeOH in CH₂Cl₂ as eluant. The product obtained was precipitated with CH₂Cl₂-Hexanes, filtered and washed with chilled CH₂Cl₂ (2 × 2 mL) to remove any traces of residual DCU to yield 85 mg (75%) of pure product. UV-vis (CH₂Cl₂): 662 (4.75×10⁴), 605 (8.55×10³), 538(9.21×10³), 506 (8.86 ×10³), 410 (9.20 ×10⁴). ¹H-NMR (CDCl₃; 400 MHz): δ 9.72, 9.44 and 8.53 (all s, 1H, meso-H); 7.74(s, 1H, ArH); 7.61(m, 1H, ArH); 7.28 (m, 1H, ArH); 7.03(m, 1H, ArH); 5.95 (q, J=6.8, 1H, 3¹-H); 5.25 (d, J=20.0, 1H, 13²-CH₂); 5.10 (d, J=20.0, 1H, 13²-CH₂); 4.65 (dd, J=4.0,12.0, 1H, OCH₂Ar); 4.50 (m, 2H, OCH₂Ar & 18-H); 4.28 (d, J=7.6, 1H, 17-H); 3.67(q, J=7.6, 2H, 8-CH₂CH₃); 3.58, 3.34 and 3.18 (all s, all 3H, for 3 × ring CH₃); 2.55–2.72 (m, 6H, succinimidyl CO(CH₂)₂CO and 17¹-H); 2.20–2.35 (m, 2H, 17²-H); 2.15 (m, 3H, 3¹-CH₃); 1.80(d, J=7.6, 3H, 18-CH₃); 1.68 (t, J=7.2, 3H, 8-CH₂CH₃); 0.02(brs, 1H, NH); -1.70 (brs, 1H, NH). HRMS for C₄₄H₄₄N₅O₆I : 865.2338 (Calculated); 866.2312 (Found, MH⁺).

Synthesis of 3-{1'-(*m*-iodobenzoyloxy)ethyl}-17²-(2-amino-2-deoxy)glucosamide-pyropheo phorbide-a (2)—To a solution of sodium methoxide (150 μL of 25% by wt) and anhydrous DMSO(2.5mL) under argon was added D-Glucosamine hydrochloride (150 mg) and reaction mixture was stirred at RT for 1.5 hrs (clear solution becomes turbid and pale in color). 0.8mL of this reaction mixture was added to 3-{1'-(3-iodobenzoyloxy)ethyl}pyropheophorbide-*a* succinimidyl ester **5** (50 mg, 0.06 mmol) and resultant reaction mixture was stirred at RT overnight. Water (10 mL) was poured into the reaction mixture and the solid that separated out was filtered and chromatographed over silica column using 10% MeOH in CH₂Cl₂ as eluant to afford 40 mg (75%) of **2**. Analytical RP HPLC (95/5: MeOH/H₂O; Symmetry): *t*_R = 8.17 min, >96%. UV-vis(CH₂Cl₂): 663 (4.75×10⁴), 606 (7.08 ×10³), 535 (8.69 ×10³), 506 (8.84 ×10³), 410 (8.89 × 10⁴). ¹H-NMR (Pyridine-*d*₅; 400 MHz): δ 10.20 (splits, 1H, meso-H); 9.96 (s, 1H, meso-H); 8.82 (s, 1H, meso-H); 8.58 (brs, 1H, CONH); 8.10 (s, 1H, ArH); 7.77 (d, J=7.6, 1H, ArH); 7.53 (d, J=8.0, 1H, ArH); 7.15 (t, J=7.8, 1H, ArH); 6.24 (t, J= 6.6, 1H, Glu-H); 5.95 (s, 1H, 3¹-H); 5.42(d, J= 20.4, 1H, 13²-CH₂); 5.18 (d, J=19.6, 1H, 13²-CH₂); 4.90 (brs, 6H, OCH₂Ar and Glu-OH); 4.48–4.85 (m, 6H, Glu-H); 4.36 (dd, J=5.8, 11.8, 1H, H-18); 4.26 (t, J=9.0, 1H, H-17); 3.79 (q, J=7.47, 2H, 8-CH₂CH₃); 3.73 (s, 3H, ring CH₃); 3.41 (s, 3H, ring CH₃); 3.29 (s, 3H, ring CH₃); 3.00–3.10 (m, 1H, 17¹-H); 2.80–2.90 (m, 1H, 17²-H); 2.65–2.75 (m, 1H, 17¹-H); 2.50–2.60 (m, 1H, 17²-H); 2.28 (d, J=6.4, 3H, 3¹-CH₃); 1.87 (d, J=6.4, 3H, 18-CH₃); 1.73 (t, J= 7.6, 3H, 8-CH₂CH₃); 0.70 (brs, 1H, NH); -1.70 (brs, 1H, NH). HRMS for C₄₆H₅₂N₅O₈I: 929.2862 (Calculated); 930.2854 (Found, MH⁺).

Synthesis of 3-{1'-(*m*-trimethylstannylbenzyloxy)ethyl}pyropheophorbide-a (7)—To a solution of **4** (70 mg, 0.09mmol) in dry THF(20 ml) were added hexamethylditin (0.1 ml, 0.48mmol) and bis-(triphenylphosphine)palladium(II)dichloride (20 mg) and the reaction mixture was stirred at RT overnight. After removing the solvent under vacuum to dryness the crude mixture was purified over silica gel column using 1% MeOH in CH₂Cl₂ as eluant to yield 40mg(55%) of compound **7**. UV-vis (CH₂Cl₂): 662 (4.75×10⁴), 606 (8.46×10³), 538 (9.16 ×10³), 507 (9.20×10³), 411 (9.57×10⁴). ¹H-NMR(CDCl₃; 400 MHz): δ 9.73, 9.40 and 8.52 (all s, 1H, meso-H); 7.42 (m, 2H, ArH); 7.34 (m, 2H, ArH); 5.98 (m, 1H, 3¹-H); 5.27 (d, J=19.6, 1H, 13²-CH₂); 5.10 (d, J=19.6, 1H, 13²-CH₂); 4.75 (dd, J=3.0, 11.2, 1H, OCH₂Ar); 4.58 (dd, J=1.8,12.0, 1H, OCH₂Ar); 4.48 (q, J=7.2, 1H, 18-H); 4.29 (d, J=8.0, 1H, 17-H); 3.64 (q, J=7.8, 2H, 8-CH₂CH₃); 3.55 (s, 3H, ring CH₃); 3.34 (s, 3H, ring CH₃); 3.15 (s, 3H, ring CH₃); 2.60–2.75 and 2.25–2.40 (m, 4H, 17¹ and 17²-H); 2.13 (m, 3H, 3¹-CH₃); 1.78 (d, J=7.2, 3H, 18-CH₃); 1.66 (t, J=7.2, 3H, 8-CH₂CH₃); 0.17 (s, 9H, Sn(CH₃)₃); 0.05 (brs, 1H, NH); -1.65 (brs, 1H, NH). HRMS for C₄₃H₅₀N₄O₄Sn: 806.2853 (Calculated); 807.2848 (Found, MH⁺).

Synthesis of 3-{1'-(*m*-trimethylstannylbenzyloxy)ethyl}pyropheophorbide-*a* succinimidyl ester (8**)**—Compound **7** (45 mg, 0.06mmol) was activated with DCC (20 mg, 0.10mmol) and *N*-hydroxysuccinimide (15 mg, 0.13mmol) in DMF (2 mL). After stirring overnight at RT, DCU was filtered off and the filtrate was concentrated and chromatographed over silica column with 2.5% MeOH in CH₂Cl₂ as eluant. The product obtained was precipitated with CH₂Cl₂-Hexanes, filtered and washed with chilled CH₂Cl₂ (2 × 2 mL) to remove any traces of residual DCU to yield 45 mg (90%) of pure product. UV-vis(CH₂Cl₂): 662 (4.75×10⁴), 606 (7.84×10³), 538 (8.28×10³), 506 (8.88×10³), 411 (9.37 ×10⁴). ¹H-NMR (CDCl₃; 400 MHz): δ 9.77 (splits, 1H, meso-H); 9.53 and 8.56 (both s, 1H, meso-H); 7.42 (m, 2H, ArH); 7.36 (m, 2H, ArH); 6.00 (q, J=6.7, 1H, 3¹-H); 5.23 (d, J=20.4, 1H, 13²-CH₂); 5.15 (d, J=19.6, 1H, 13²-CH₂); 4.77 (dd, J=5.2,11.6, 1H, OCH₂Ar); 4.60 (dd, J=1.8,11.8, 1H, OCH₂Ar); 4.49–4.55 (m, 1H, 18-H); 4.43 (d, J=9.2, 1H, 17-H); 3.72 (q, J=8.0, 2H, 8-CH₂CH₃); 3.68, 3.37 and 3.17 (all s, all 3H, for 3 × ring CH₃); 2.87 (brs, 6H, succinimidyl CO (CH₂)₂CO and 17¹-H); 2.56–2.63 and 2.25–2.35 (m, 2H, 17²-H); 2.15 (dd, J=3.6, 6.4, 3H, 3²-CH₃); 1.82(d, J=7.2, 3H, 18-CH₃); 1.70 (t, J=7.2, 3H, 8-CH₂CH₃); 0.44 (brs, 1H, NH); 0.18 (s, 9H, Sn(CH₃)₃); -1.70 (brs, 1H, NH). HRMS for C₄₇H₅₃N₅O₆Sn: 903.3017 (Calculated); 904.3009 (Found, MH⁺).

Synthesis of 3-{1'-(*m*-trimethylstannylbenzyloxy)ethyl}-17²-(2-amino-2-deoxy) glucosa-mide-pyropheophorbide-*a* (9**)**—It was synthesized using the respective starting material **10** by following the procedure reported for **2**. Yield: (75%). Analytical RP HPLC (95/5: MeOH/H₂O; Symmetry): *t*_R = 10.51 min, >96%. UV-vis (MeOH/CH₂Cl₂): 662 (4.75×10⁴), 605 (8.62×10³), 539 (9.24×10³), 507 (8.93×10³), 410 (9.07×10⁴). ¹H-NMR (Pyridine-*d*₅; 400 MHz): δ 10.24 (splits, 1H, meso-H); 9.95 (s, 1H, meso-H); 8.82(s, 1H, meso-H); 8.58 (brs, 1H, amidic NH); 7.78 (s, 1H, ArH); 7.67 (m, 1H, ArH); 7.60 (m, 1H, ArH); 7.51 (m, 1H, ArH); 6.28 (m, 1H, 3¹-H); 5.35–5.45 (m, 2H, 13²-CH₂, Glu-H); 5.18 (d, J=20.0, 1H, 13²-CH₂); 4.80–5.1 (brs, 7H, OCH₂Ar, Glu-H, Glu-OH); 4.69 (m, 1H, Glu-H); 4.62 (m, 2H, Glu-H); 4.50(m, 2H, Glu-H); 4.36 (m, 1H, 18-H); 4.26(m, 1H, 17-H); 3.79 (q, J=7.5, 2H, 8-CH₂CH₃); 3.73 (s, 3H, ring CH₃); 3.44 (d, J=6.4, 3H, ring CH₃); 3.25 (s, 3H, ring CH₃); 3.00–3.10 (m, 1H, 17¹-H); 2.80–2.90 (m, 1H, 17²-H); 2.65–2.75 (m, 1H, 17¹-H); 2.50–2.60 (m, 1H, 17²-H); 2.30 (d, J=6.4, 3H, 3¹-CH₃); 1.87 (d, J=6.4, 3H, 18-CH₃); 1.74 (t, J= 7.6, 3H, 8-CH₂CH₃); 0.73 (brs, 1H, NH); 0.23 (s, 9H, Sn(CH₃)₃); -1.70(brs, 1H, NH). HRMS for C₄₉H₆₁N₅O₈Sn: 967.3541 (Calculated); 968.3534 (Found, MH⁺).

Synthesis of 3-{1'-(*m*-iodobenzyloxy)ethyl}-17²-(1-amino-1-deoxy) tetraacetogalactosamide- pyropheophorbide-*a* (6**)**—Compound **4** (30 mg, 0.04mmol), tetraacetogalactosamine (30 mg, 0.08mmol) and PyBOP(26 mg, 0.05mmol) were added to anhydrous DMF (3 mL) under nitrogen and reaction mixture was stirred at RT overnight. DMF was removed under vacuum and crude obtained was purified over silica preparative TLC plate using 5% MeOH in CH₂Cl₂ as eluant. Yield: 25 mg (60%). ¹H-NMR (CDCl₃; 400 MHz): δ 9.78 (s, 1H, meso-H); 9.54 (s, 1H, meso-H); 8.56 (s, 1H, meso-H); 7.75 (s, 1H, ArH); 7.65 (d, J=7.2, 1H, ArH); 7.32 (d, J=7.6, 1H, ArH); 7.07 (dt, J=0.8, 7.8, 1H, ArH); 6.06 (dd, J=4.0, 9.2, 1H, CONH); 6.01 (q, J= 6.8, 1H, 3¹-H); 5.40 (d, J=3.2, 1H, Gal-H); 5.29 (d, J=19.2, 1H, 13²-CH₂); 5.05–5.25 (m, 3H, 13²-H & Gal-H); 4.95 (dt, J=2.4, 10.2, 1H, Gal-H); 4.72 (dd, J=3.2,12.0, 1H, Gal-H); 4.58 (dd, J=1.8,11.8, 1H, Gal-H); 4.50 (dq, J=1.2,6.8, 1H, 18-H); 4.38 (m, 1H, 17-H); 4.05 (m, 2H, OCH₂Ar); 3.99 (m,1H, Gal-H); 3.72 (q, J=7.6, 2H, 8-CH₂CH₃); 3.67 (s, 3H, ring CH₃); 3.40 (splits, 3H, ring CH₃); 3.23 (splits, 3H, ring CH₃); 2.65–2.75 (m, 1H, 17¹-H); 2.30–2.45 (m, 2H, 17²-H & 17¹-H); 2.19 (dd, J=3.0, 6.8, 3H, 3¹-CH₃); 2.06 (brs, 4H, 17²-H & COCH₃); 2.00 (s, 3H, COCH₃); 1.96 (s, 3H, COCH₃); 1.92 (s, 3H, COCH₃); 1.83 (d, J= 7.6, 3H, 18-CH₃); 1.72 (t, J=7.6, 3H, 8-CH₂CH₃); 0.45 (brs, 1H, NH); -1.70 (brs, 1H, NH). HRMS for C₅₄H₆₀N₅O₁₂I: 1097.3284 (Calculated); 1098.3277 (Found, MH⁺).

Synthesis of {1'- (*m*-iodobenzoyloxy)ethyl}-17²-(1-amino-1-deoxy)

galactosamide-pyro pheophorbide-a (3)—To a solution of 1'- (3-iodobenzoyloxy ethyl)-17²-(1-amino-1-deoxy)tetraacetogalactos amide-pyropheophorbide-*a* (**6**) (22 mg, 0.02mmol) in dry CH₂Cl₂ (5 ml) and dry MeOH (0.5 mL) under nitrogen, sodium methoxide (100 μL) was added and the reaction mixture was stirred for 20 minutes at RT. The reaction mixture was neutralized with resin and filtered. The filtrate was removed under vacuum and purified by passing through a short silica column using 10% MeOH in CH₂Cl₂ as eluant to yield 15 mg (80%) of **3**. Analytical RP HPLC (95/5: MeOH/H₂O; Symmetry): *t*_R = 8.02 min, >96%. UV-vis (CH₂Cl₂): 662 (4.75×10⁴), 606 (8.75 ×10³), 538 (9.30 ×10³), 507 (8.96 ×10⁴), 411 (8.29 × 10⁴). ¹H-NMR (Pyridine-*d*₅; 400 MHz): δ 10.20 (d, J=9.6, 1H, meso-H); 9.94 (s, 1H, meso-H); 9.60 (d, J=8.8, 1H, meso-H); 8.80 (s, 1H, CONH); 8.08 (s, 1H, ArH); 7.75 (d, J=7.6, 1H, ArH); 7.51 (d, J=6.8, 1H, ArH); 7.12 (t, J=7.4, 1H, ArH); 6.23 (t, J=6.8, 1H, Gal-H); 5.92 (t, J= 8.6, 1H, 3¹-H); 5.36 (d, J=20.0, 1H, 13²-CH₂); 5.16 (d, J=20.0, 1H, 13²-CH₂); 4.70–4.90 (m, 6H, OCH₂Ar, Gal-OH); 4.54 (d, J=7.2, 2H, Gal-H); 4.47 (brs, 1H, 18-H); 4.37 (brs, 3H, Gal-H); 4.14 (m, 2H, 17-H & Gal-H); 3.79 (d, J=7.2, 2H, 8-CH₂CH₃); 3.74 (s, 3H, ring CH₃); 3.42 (s, 3H, ring CH₃); 3.29 (s, 3H, ring CH₃); 2.90–3.00 (m, 1H, 17¹-H); 2.60–2.80 (m, 2H, 17¹-H & 17²-H); 2.35–2.45 (m, 1H, 17²-H); 2.28 (d, J=5.6, 3H, 3¹-CH₃); 1.82 (d, J= 6.4, 3H, 18-CH₃); 1.73 (t, J=6.8, 3H, 8-CH₂CH₃); 0.71 (brs, 1H, NH); -1.46(brs, 1H, NH). HRMS for C₄₆H₅₂N₅O₈I: 929.2862 (Calculated); 930.2806 (Found, MH⁺).

Synthesis of 3-{1'- (*m*-trimethylstannylbenzyloxy)ethyl}-17²-(1-amino-1-deoxy) tetraaceto- galactosamide-pyropheophorbide-a (10)

—The title compound was synthesized by following the procedure described for **6** from the respective starting material **7**. Yield: 55%. ¹H-NMR (CDCl₃; 400 MHz): δ 9.77 (s, 1H, meso-H); 9.52(s, 1H, meso-H); 8.54 (s, 1H, meso-H); 7.43 (m, 2H, ArH); 7.35 (m, 2H, ArH); 5.95–6.05 (m, 2H, CONH & 3¹-H); 5.37 (d, J=3.2, 1H, Gal-H); 5.26 (d, J=18.8, 1H, 13²-CH₂); 5.18 (d, J=18.8, 1H, 13²-CH₂); 5.02–5.10 (m, 2H, Gal-H); 4.90–5.00 (m, 1H, Gal-H); 4.78 (dd, J=5.8,11.4, 1H, Gal-H); 4.61 (d, J=11.6, 1H, Gal-H); 4.48 (q, J=7.6, 1H, H-18); 4.36 (m, 1H, H-17); 4.00–4.10 (m, 2H, OCH₂Ar); 3.95–4.00 (m, 1H, Gal-H); 3.70 (q, J=7.6, 2H, 8-CH₂CH₃); 3.66 (s, 3H, ring CH₃); 3.37 (splits, 3H, ring CH₃); 3.17 (s, 3H, ring CH₃); 2.60–2.75 (m, 1H, 17¹-H); 2.30–2.45 (m, 2H, 17²-H & 17¹-H); 2.12–2.18 (m, 4H, 17²-H & 3¹-CH₃); 2.04 (s, 3H, COCH₃); 1.98 (s, 3H, COCH₃); 1.93 (s, 3H, COCH₃); 1.90 (s, 3H, COCH₃); 1.81 (d, J= 7.2, 3H, 18-CH₃); 1.70 (t, J=7.6, 3H, 8-CH₂CH₃); 0.45 (brs, 1H, NH); 0.19 (s, 9H, Sn(CH₃)₃); -1.69 (brs, 1H, NH). HRMS for C₅₇H₆₉N₅O₁₂Sn: 1135.3964 (Calculated); 1136.3786 (Found, MH⁺).

Synthesis of 3-devinyl-3-{1'-(*m*-trimethylstannylbenzyloxy)ethyl}-17²-(1-amino-1-deoxy) galactosamide -pyropheophorbide-a (11)

—The title compound was synthesized by following the procedure described for **3** by using the respective starting material **10**. Yield: 55%. Analytical RP HPLC (95/5: MeOH/H₂O; Symmetry): *t*_R = 9.88 min, >96%. UV-vis(CH₂Cl₂): 661(4.75×10⁴), 605(8.92 ×10³), 537(9.42 ×10³), 505(9.16 ×10⁴), 408(8.33 × 10⁴). ¹H-NMR (Pyridine-*d*₅; 400 MHz): δ 10.24 (d, J=9.6, 1H, meso-H); 9.95 (s, 1H, meso-H); 9.58 (d, J=9.2, 1H, meso-H); 8.81 (d, J=3.2, 1H, CONH); 7.77(s, 1H, ArH); 7.66 (m, 1H, ArH); 7.60 (m, 1H, ArH); 7.51 (m, 1H, ArH); 6.28 (m, 1H, Gal-H); 5.92 (t, J=8.8, 1H, 3¹-H); 5.36 (d, J=20.0, 1H, 13²-CH₂); 5.16 (d, J=20.4, 1H, 13²-CH₂); 5.00 (d, J=11.6, 1H, Gal-H); 4.84 (brs, 5H, Gal-H & Gal-OH); 4.54 (m, 2H, Gal-H); 4.47 (m, 1H, 18-H); 4.37 (m, 3H, OCH₂Ar & Gal-H); 4.14 (m, 2H, 17-H, Gal-H); 3.79 (d, J=7.6, 2H, 8-CH₂CH₃); 3.75 (s, 3H, ring CH₃); 3.44 (splits, 3H, ring CH₃); 3.24 (s, 3H, ring CH₃); 2.90–3.00 (m, 1H, 17¹-H); 2.60–2.80 (m, 2H, 17²-H & 17¹-H); 2.35–2.45 (m, 1H, 17²-H); 2.29 (d, J=6.0, 3H, 3¹-CH₃); 1.82 (d, J= 6.8, 3H, 18-CH₃); 1.73 (t, J=7.4, 3H, 8-CH₂CH₃); 0.75 (brs, 1H, NH); 0.23 (s, 9H, Sn (CH₃)₃); -1.42 (d, J=5.6, 1H, NH). HRMS for C₄₉H₆₁N₅O₈Sn : 967.3541 (Calculated); 968.3452 (Found, MH⁺).

Radioactive Labeling

^{124}I -analogs of **2** and **3** were prepared from the corresponding trimethylstannyl analogs **9** and **11** respectively by following the procedure as described below for ^{124}I analog of compound **1**.

Synthesis of ^{124}I - analog of 3-{1'- (m-iodobenzoyloxy)ethyl}pyropheophorbide-a methyl ester (1**)**—The trimethyltin analog **12** (50 Pg) was dissolved in 50 Pl of 5% acetic acid in methanol. 100 Pl of 5% acetic acid in methanol was added to Na^{124}I in 10 Pl of 0.1N NaOH. The two solutions were mixed and an IODOGEN[®] bead (Pierce Biotechnology, Inc., Rockford, IL 61106) was added. The reaction mixture was incubated at room temperature for 15 minutes, iodobead was removed and the reaction mixture was injected on an HPLC column (Phenomenex Maxsil C8 5P), which was eluted with an isocratic 90/10: MeOH/H₂O at a flow rate of 1 ml/min. The UV detector was set at 254nm wavelength. The labeled product (**1**) eluted at 10.53 min (Supplementary Data) was collected and the solvent was evaporated to dryness under stream of N₂ at 60°C. The product was formulated in saline containing 10% ethanol for *in vivo* experiments. RadioTLC confirmed the radiochemical purity (>95%) of the product. A standard curve was generated between peak area versus mass by injecting a known mass of carrier **1** onto the column. The mass associated with the labeled product was calculated by relating the peak area of UV absorbance peak of **1** in the labeled product to the standard curve. The specific activity was obtained by dividing the activity of the labeled product collected by the calculated mass in micromoles. Specific activity of radiolabeled product for 5 runs was in the range of 2.1 +/- 1.4 (9) Ci/ μmol . The radiochemical yield of the reaction was 20%.

HPLC conditions for compound 2: Eluant: MeOH/water, 95:5; wavelength, 254 nm; flow rate, 1 ml/min; retention time for the ^{124}I -derivative, 9 min, retention time for the intermediate trimethyl tin derivatibe, 11 min. Column: Symmetry, C18. Radiochemical yield: 36%. Specific activity 4.3 Ci/ μmol .

HPLC conditions for compound 3: Eluant: MeOH/water, 95:10; wavelength, 254 nm; flow rate, 1 ml/min; retention time, ^{124}I -derivative, 22.8 mn, retention time for the intermediate trimethyl tin derivatibe, 27.8 min. Column: Maxsil. Radiochemical yield: 14%. Specific activity 3.2 Ci/ μmol .

In vivo photosensitizing efficacy (Kaplan Meier Plot)—The female C3H/HeJ mice were intradermally injected with 2×10^5 RIF cells in 30 ml HBSS without Ca²⁺ and Mg²⁺ on the flank and tumors were grown until they reached 4–5 mm in diameter. The day before laser light treatment, all hair was removed from the inoculation site and the mice were injected intravenously with varying photosensitizers' doses. At 24 hours post-injection, the mice were restrained without anesthesia in plastic holders and then treated with laser light from a dye laser tuned to emit drug-activating wavelengths. The treatment parameters consisted of an irradiated area of 1 cm², a fluence rate of 75 mW/cm² for a dose of 135 J/cm². The mice were observed daily for signs of weight loss, necrotic scabbing, or tumor re-growth. If tumor growth appeared, the tumors were measured using two orthogonal measurements L and W (perpendicular to L) and the volumes were calculated using the formula $V = (L \times W^2)/2$ and recorded. Mice were considered cured if there was no sign of tumor re-growth by day 60 post-PDT treatment.

PET Imaging—Mice were imaged in the microPET FOCUS 120[®], a dedicated 3D small-animal PET scanner (Concorde Microsystems Incorporated) at State University of New York at Buffalo under the Institutional Animal Care and Use Committee (IACUC) guidelines. The C3H mice were subcutaneously injected with 3×10^5 RIF cells in 30 μl complete α - MEM (into the axilla) and tumors were grown until they reached 4–5 mm in diameter (approximately

5 days). All tumored C₃H mice were injected via the tail vein with 72–200 μ Ci of 1–3 and after 24, 48, 72 and 96h post injection the mice were anesthetized by inhalation of isoflurane/oxygen, placed head first prone for imaging and the acquisition time was set for 30 minutes. Radioiodine uptake by thyroid or stomach was not blocked. All mice going through imaging were marked with a cross-line on the back to provide a reference landmark for consistently positioning them in a series of imaging studies. The acquired data were rebinned with FORE algorithm (20) and reconstructed with 2D OSEM algorithm. The dead-time and singles-based random coincidence corrections were applied to all the PET studies. The RUV results were calculated from PET images with attenuation and scatter corrections, in addition to the dead-time and random coincidence corrections. The transmission scan for attenuation correction was carried out with a rotating ⁵⁷Co point source.

Biodistribution studies

Gamma well counter—All studies were performed as per IACUC guidelines. The mice (3–4 mice for each compound/time point) were injected with 15–200 μ Ci of 1–3 via tail vein and were sacrificed at 24, 48, 72 and 96 h post injection, blood and body organs (tumor, heart, liver, spleen, kidney, lung, muscle, gut and stomach) removed immediately. After weighing, the amount of radioactivity in the tumor (50–150 mg), body organs and blood was measured by a gamma well counter. Radioactivity uptake was calculated as the percentage of the injected dose/gram of the tissue (%ID/g). Statistical analyses and data (%ID/g vs. time point) were plotted using Microsoft Excel.

Supplementary Material

Refer to Web version on PubMed Central for supplementary material.

Acknowledgments

The financial support from the NIH (CA 114053, CA127369, CA55791), Roswell Park Alliance Foundation and the shared resources of the RPCI support grant (P30CA16056) is highly appreciated.

Keywords

PDT	Photodynamic Therapy
PET	Positron-Emission Tomography
FDG	Fluoro Deoxy-Glucose
MR	Magnetic Resonance
ID	Injected Dose
RUV	Relative Uptake Value
PEG	Poly Ethylene Glycol

References

1. Massoud TF, Gambhir SS. Molecular imaging in living subjects: Seeing fundamental biological processes in a new light. *Genes & Development* 2003;17:545–580. [PubMed: 12629038]
2. Gambhir SS, Czernin J, Schwimmer J, Silverman DHS, Coleman RE, Phelps ME. A tabulated summary of the FDG PET literature. *J Nucl Med* 2001;42(suppl):1S–93S. [PubMed: 11483694]
3. Abouzed MM, Crawford ES, Nabi HA. ^{18}F -FDG Imaging: Pitfalls and Artifacts. *J Nucl Med Technol* 2005;33:145–155. [PubMed: 16145222]
4. (a) Pentlow KS, Graham MC, Lambrecht RM, Daghighian F, Bacharach SL, Bendriem B, Finn RD, Jordon K, Kalaigian H, Karp JS, Robeson WR, Larson SM. Quantitative imaging of iodine-124 with PET. *J Nucl Med* 1996;37:1557–1562. [PubMed: 8790218] (b) Trotter DEG, Manjeshwar RM, Doss M, Shaller C, Robinson MK, Tandon R, Adams GP, Adler LP. Quantitation of small-animal ^{124}I -activity distributions using a clinical PET/CT scanner. *J Nucl Med* 2004;45:1237–1244. [PubMed: 15235072]
5. Verel I, Vissser GWM, vanDongen GAMS. The promise of immuno-PET in radioimmunotherapy. *J Nucl Med* 2005;46:164S–171S. [PubMed: 15653665] (b) Bennett JJ, Tjuvajev J, Johnson P, Doubrovin M, Akhurst T, Malholtra S, Hackman T, Balatoni J, Finn R, Larson SM, Federoff H, Blasberg R, Fong YM. Positron emission tomography imaging for herpes virus infection: Implications for oncolytic viral treatments of cancer. *Nature Medicine* 2001;7:859–863. (c) Doubrovin M, Ponomarev V, Beresten T, Balatoni J, Bornmann W, Finn R, Humm J, Larson S, Sadelain M, Blasberg R, Tjuvajev JG. Imaging transcriptional regulation of p53-dependent genes with positron emission tomography in vivo. *Proc Natl Acad Sci USA* 2001;98:9300–9305. [PubMed: 11481488] (d) Jacobs A, Voges J, Reszka R, Lercher M, Gossmann A, Kracht L, Kaestle C, Wagner R, Wienhard K, Heiss WD. Positron-emission tomography of vector-mediated gene expression in gene therapy for gliomas. *Lancet* 2001;358:727–729. [PubMed: 11551583] (e) Divgi CR, Pandit-Taskar N, Jungbluth AA, Reuter VE, Gonen M, Ruan S, Pierre C, Nagel A, Pryma DA, Humm J, Larson SM, Old LJ, Russo P. Preoperative characterization of clear-cell renal carcinoma using iodine-124 labelled antibody chimeric G250 (124I-cG250) and PET in patients with renal masses: a phase I trial. *Lancet Oncol* 2007;8:304–310. [PubMed: 17395103]
6. (a) Henderson BW, Dougherty TJ. How does photodynamic therapy work? *Photochem Photobiol* 1992;55:145–157. [PubMed: 1603846] (b) Dougherty TJ, Gomer CJ, Henderson BW, Jori G, Kessel D, Korbelik M, Moan J, Peng Q. Photodynamic therapy. *J Natl Cancer Inst* 1998;90:889–905. [PubMed: 9637138]
7. Dolmans DE, Fukumura D, Jain RK. Photodynamic therapy for cancer. *Nat Rev Cancer* 2003;3:380–387. [PubMed: 12724736]
8. (a) Pandey RK, Sumlin AB, Constantine S, Aoudia M, Potter WR, Bellnier DA, Henderson BW, Rodgers MA, Smith KM, Dougherty TJ. Alkyl ether analogs of chlorophyll-a derivatives: Part 1. Synthesis, photophysical properties and photodynamic efficacy. *Photochem Photobiol* 1996;64:194–204. [PubMed: 8787014] (b) Henderson BW, Bellnier DA, Greco WR, Sharma A, Pandey RK, Vaughan LA, Weishaupt KR, Dougherty TJ. An in vivo quantitative structure-activity relationship for a congeneric series of pyropheophorbide derivatives as photosensitizers for photodynamic therapy. *Cancer Res* 1997;57:4000–4007. [PubMed: 9307285] (c) Dougherty TJ, Sumlin AB, Greco WR, Weishaupt KR, Vaughan LA, Pandey RK. The role of the peripheral benzodiazepine receptor in photodynamic activity of certain pyropheophorbide ether photosensitizers: Albumin site II as a surrogate marker for activity. *Photochem Photobiol* 2002;76:91–97. [PubMed: 12126312] (d) Bellnier DA, Greco WR, Loewen GM, Bellnier DA, Nava H, Oseroff AR, Pandey RK, Tsuchida T, Dougherty TJ. Population pharmacokinetics of the photodynamic therapy agent 2-[1-Hexyloxyethyl]-2-devinyl Pyropheophorbide-a in Cancer Patients. *Cancer Res* 2003;63:1806–1813. [PubMed: 12702566] (e) Bellnier DA, Greco WR, Nava H, Loewen GM, Oseroff AR, Dougherty TJ. Mild skin photosensitivity in cancer patients following injection of Photochlor [2-(1'-hexyloxyethyl)-2-devinyl pyropheophorbide-a; HPPH] for photodynamic therapy. *Cancer Chemotherapy and Pharmacology* 2006;57:40–45. [PubMed: 16001178]
9. (a) Westermann P, Glanzmann T, Andrejevic S, Braichotte DR, Forrer M, Wagnieres GA, Monnier P, Van DBH, Mach JP, Folli S. Long circulating half-life and high tumor selectivity of the photosensitizer meta-tetrahydroxyphenylchlorin conjugated to polyethylene glycol in nude mice grafted with a human colon carcinoma. *Int J Cancer* 1998;76:842–850. [PubMed: 9626351] (b) Vrouenraets MB, Visser

- GWM, Stewart FA, Vrouenraets MB, Visser GWM, Stewart FA, Stigter M, Oppelaar H, Postmus PE, Snow GB, van Dongen GAMS. Development of meta-tetrahydroxyphenylchlorin-monoclonal antibody conjugates for photoimmunotherapy. *Cancer Research* 1999;59:1505–1513. [PubMed: 10197621] (c) Whelpton R, Michael-Titus AT, Jamdar RP, Abdillahi K, Grahn MF. Distribution and excretion of Radiolabeled Temoporfin in a Murine Tumor Model. *Photochemistry and Photobiology* 1996;63:885–891. [PubMed: 8992509] (d) Wilson BC, VanLier JE. Radiolabelled photosensitizers for tumor imaging and photodynamic therapy. *Journal of Photochemistry and Photobiology, B: Biology* 1989;3:459–463.
10. (a) Chen Y, Gryshuk A, Achilefu S, Ohulchansky T, Potter W, Zhong TX, Morgan J, Chance B, Prasad PN, Henderson BW, Oseroff A, Pandey RK. A novel approach to a bifunctional photosensitizer for tumor imaging and phototherapy. *Bioconjugate Chem* 2005;16:1264–1274. (b) Pandey SK, Chen Y, Zawada RH, Oseroff A, Pandey RK. Utility of tumor-avid photosensitizers in developing bifunctional agents for tumor imaging and/or phototherapy. *Proceedings of SPIE* 2006;6139:613905/1–613905/7.
 11. Ma B, Li G, Kanter P, Lamonica D, Grossman Z, Pandey RK. Bifunctional HPPH-N₂S₂ Tc-99m conjugates as tumor imaging agents: synthesis and biodistribution studies. *Journal of Porphyrins and Phthalocyanines* 2003;1:500–507.
 12. Pandey SK, Gryshuk AL, Sajjad M, Zheng X, Chen Y, Abouzeid MM, Morgan J, Charamisinau I, Nabi HA, Oseroff A, Pandey RK. Multimodality agents for tumor imaging (PET, Fluorescence) and photodynamic therapy. A possible “See and Treat” approach. *J Med Chem* 2005;48:6286–6294. [PubMed: 16190755]
 13. (a) Zheng G, Graham A, Shibata M, Missert JR, Oseroff AR, Dougherty TJ, Pandey RK. Synthesis of beta-galactose-conjugated chlorins derived by enyne metathesis as galectin-specific photosensitizers for photodynamic therapy. *J Org Chem* 2001;66:8709–8716. [PubMed: 11749598] (b) Li G, Pandey SK, Graham A, Dobhal MP, Mehta R, Chen YH, Gryshuk A, Rittenhouse-Olson K, Oseroff A, Pandey RK. Functionalization of OEP-based benzochlorins to develop carbohydrate-conjugated photosensitizers. Attempt to target beta-galactoside-recognized proteins. *J Org Chem* 2004;69:158–172. [PubMed: 14703392] (c) Pandey SK, Zheng X, Morgan J, Missert JR, Liu TH, Shibata M, Bellnier DA, Oseroff AR, Henderson BW, Dougherty TJ, Pandey RK. Purpurinimide carbohydrate conjugates: Effect of the position of the carbohydrate moiety in photosensitizing efficacy. *Molecular Pharmaceutics* 2007;4:448–464. [PubMed: 17373821] (d) Haubner R, Kuhnast B, Mang C, Weber WA, Kessler H, Wester HJ, Schwaiger M. ¹⁸F-Galacto-RGD: Synthesis, radiolabeling, metabolic stability, and radiation dose estimates. *Bioconjugate Chem* 2004;15:61–69.
 14. Speizer L, Haugland R, Kutchai H. Asymmetric transport of a fluorescent glucose analogue by human erythrocytes. *Biochem Biophys Acta* 1985;815:75–84. [PubMed: 4039191]
 15. Zhang M, Zhang Z, Blessington D, Li H, Busch TM, Madrak V, Miles J, Chance B, Glickson JD, Zheng G. Pyropheophorbide 2-deoxyglucosamide: a new photosensitizer targeting glucose transporters. *Bioconjugate Chem* 2003;14:709–714.
 16. Zheng, X.; Pandey, R. K. et al, Unpublished results.
 17. Zheng G, Potter WR, Camacho SH, Missert JR, Wang GS, Bellnier DA, Henderson BW, Rodgers MAJ, Dougherty TJ, Pandey RK. Synthesis, Photophysical properties, tumor uptake, and preliminary in vivo photosensitizing efficacy of a homologous series of 3-(1'-alkyloxy)ethyl-3-devinylpurpurin-18-N-alkylimides with variable lipophilicity. *J Med Chem* 2001;44:1540–1559. [PubMed: 11334564]
 18. Smith KM, Golf DA, Simpson DA. Meso substitution of chlorophyll derivatives: direct route for transformation of bacteriopheophorbides *d* into bacteriopheophorbides. *c J Am Chem Soc* 1985;107:4941–4954.
 19. Sajjad M, Bars E, Nabi HA. Optimization of ¹²⁴I production via ¹²⁴Te(p,n)¹²⁴I reaction. *App Radiat Isot* 2006;64:965–970.
 20. Defrise M, Kinahan PE, Townsend DW, Michel C, Sibomana M, Newport DF. Exact and approximate rebinding algorithms for 3-D PET data. *IEEE Trans Med Imaging* 1997;16(2):145–58. [PubMed: 9101324]

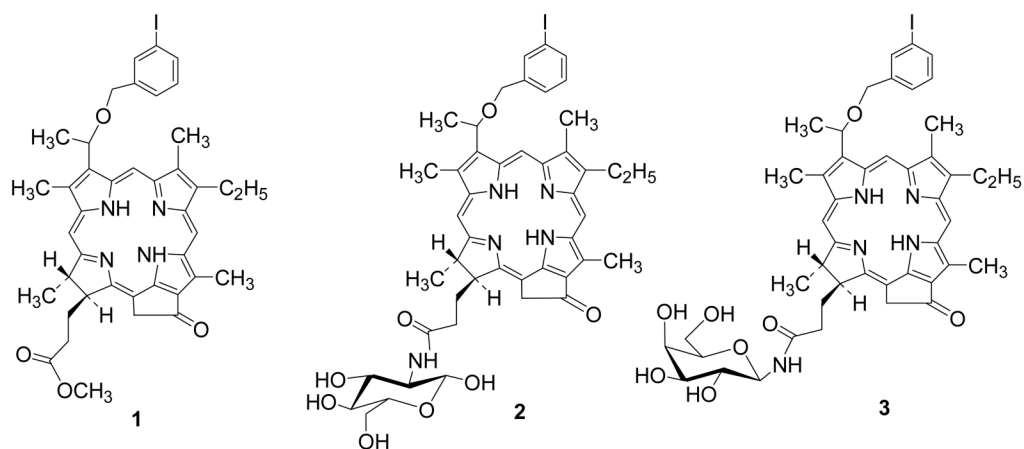


Figure 1.
Chemical structures of the lead compound **1** and its corresponding glucose **2** and galactose **3** conjugate.

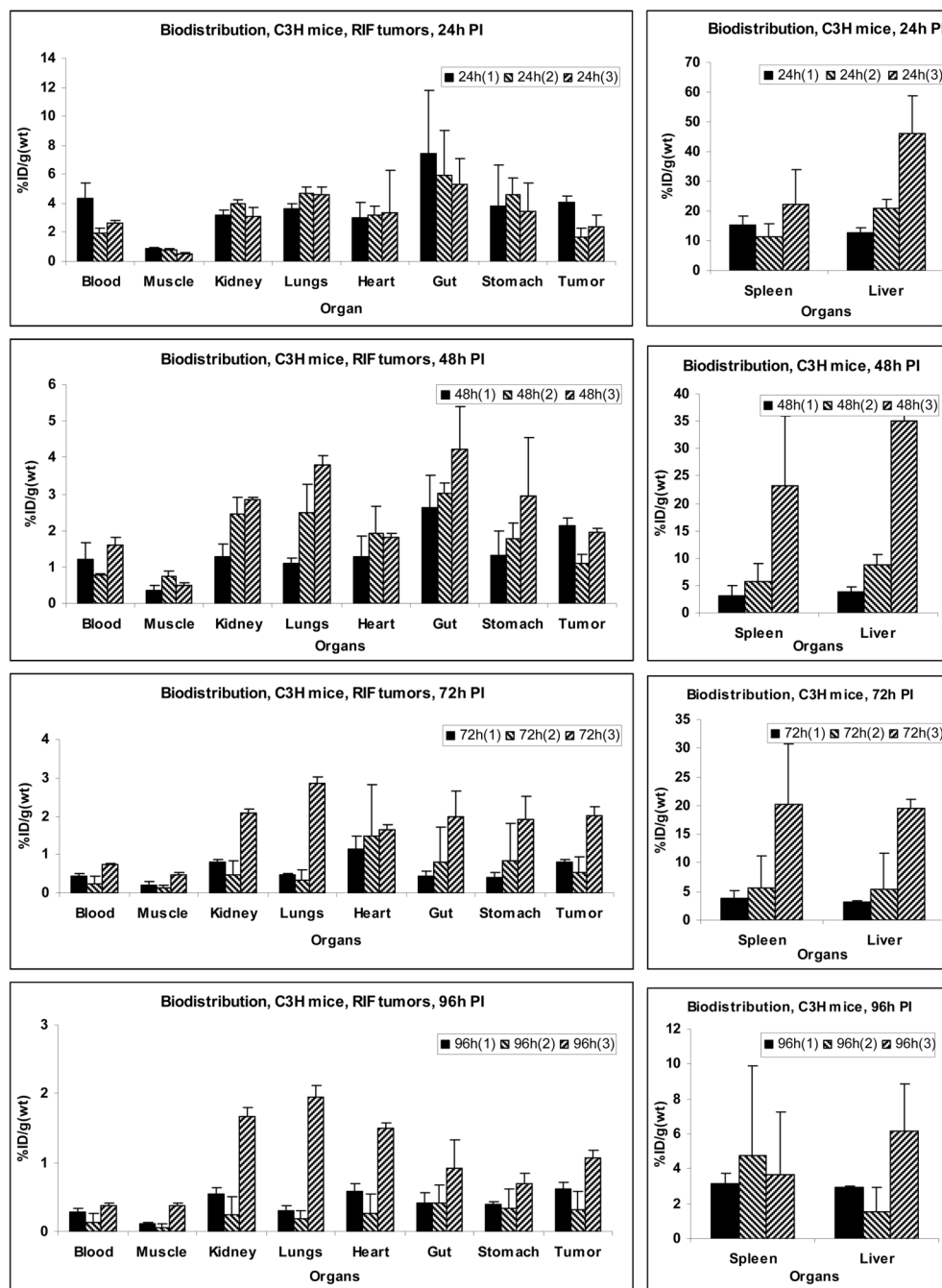


Figure 2. Comparative *in vivo* biodistribution of **1**, **2** and **3** at selected time points in C3H mice implanted with RIF tumors. Values represent mean from 3 or 4 mice/group.

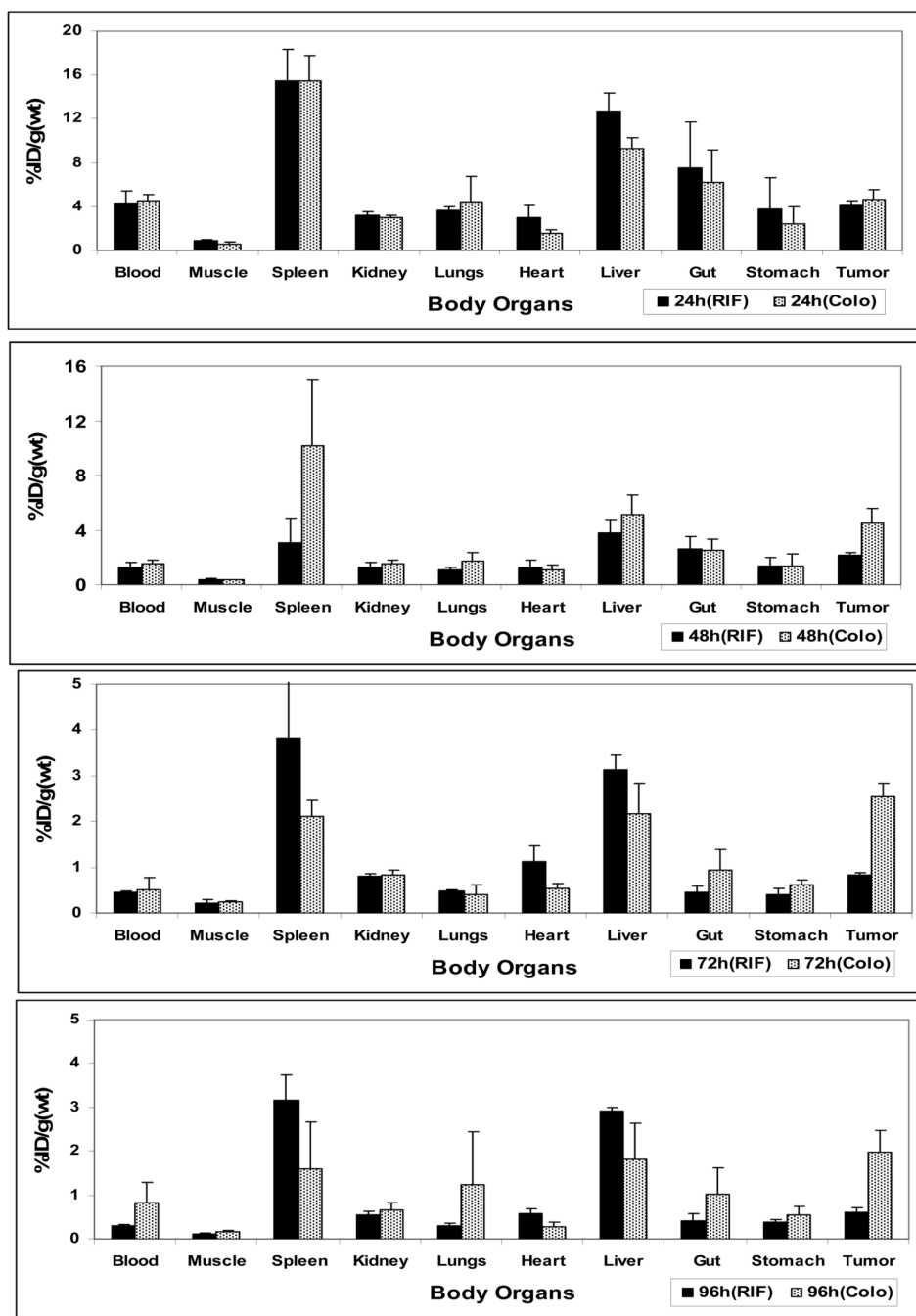


Figure 3. Comparative *in vivo* biodistribution of **1** in C3H mice (RIF tumors) and BALB/c (Colon- 26 tumors) at selected time points. Values represents mean from 3 or 4 mice/group.

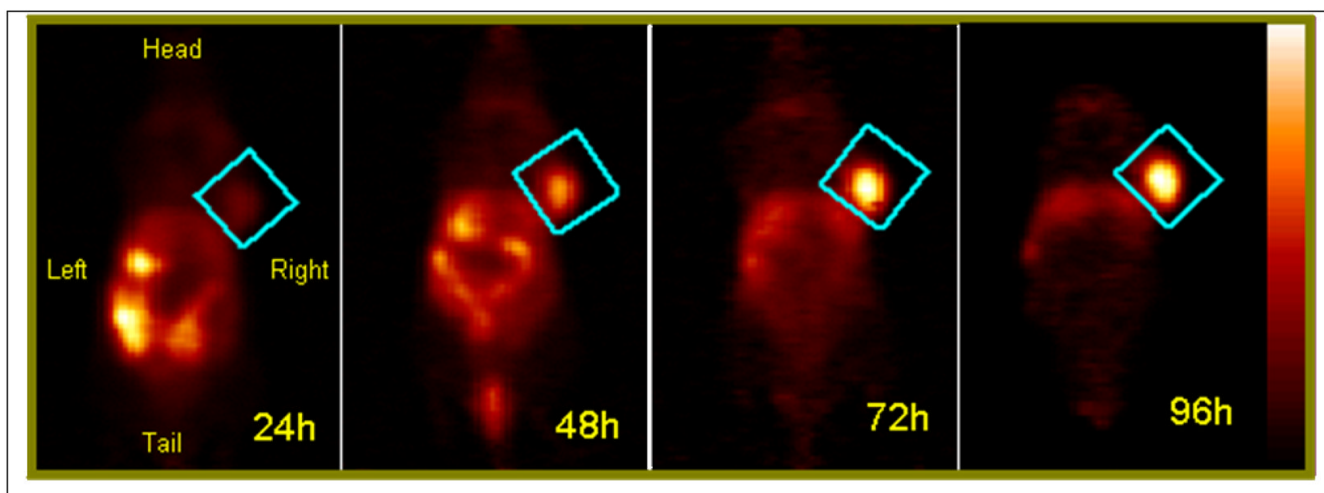


Figure 4.

The coronal view PET images of a BALB/c mice bearing Colon-26 tumors on the right shoulder injected with 150 μCi ^{124}I - of compound **1**. The studies were acquired for 30 min at 24 h, 48 h, 72 h and 96 h post injection. The tumor was identified to be within the region defined by a cylinder indicated by the blue rectangle in each image. The color palette (shown on the right) for each image shown was scaled to the min/max of each dataset.

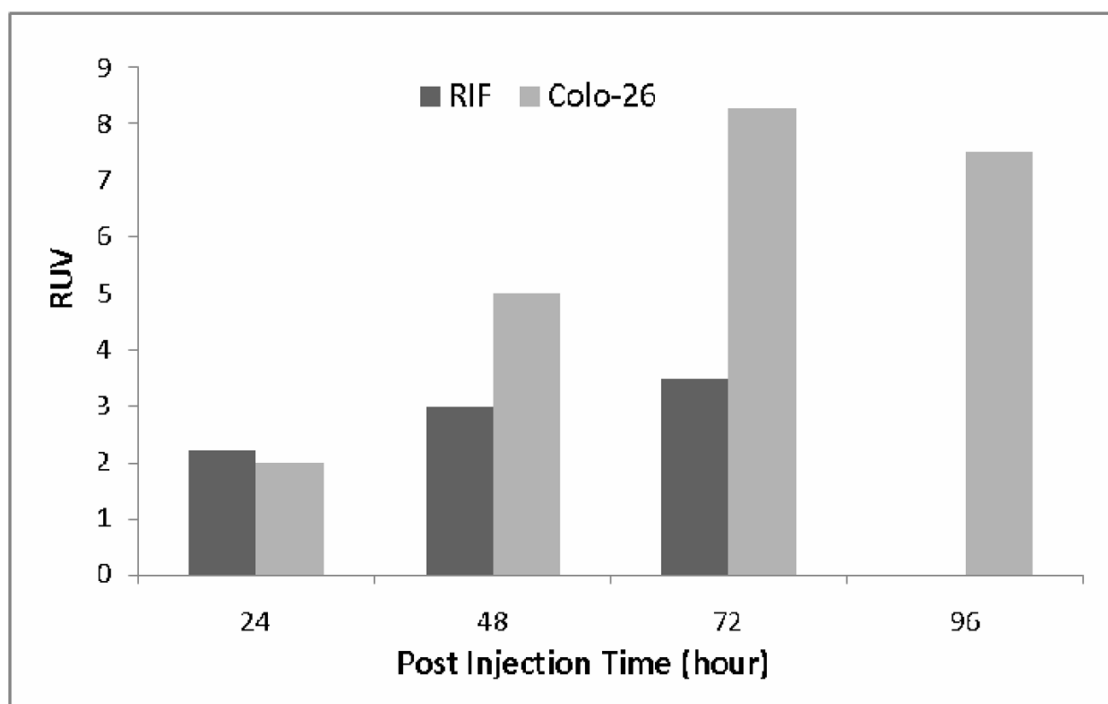


Figure 5. Comparison of RIF and Colon-26 tumor RUV with ^{124}I -compound 1.

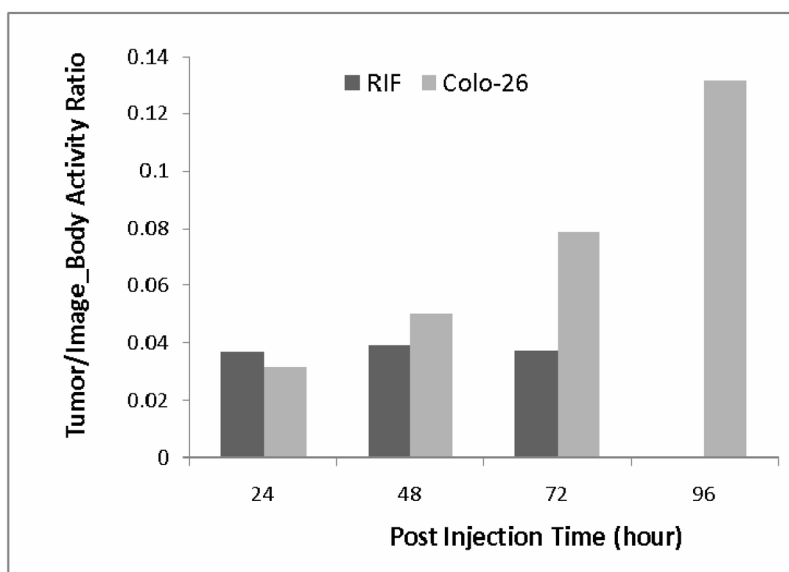


Figure 6. Comparison of RIF and Colon-26 tumor activity to whole body activity ratio over time with ^{124}I -compound **1**. Both activity values were directly derived from images. [Note the increasing activity in the Colo-26] tumor.

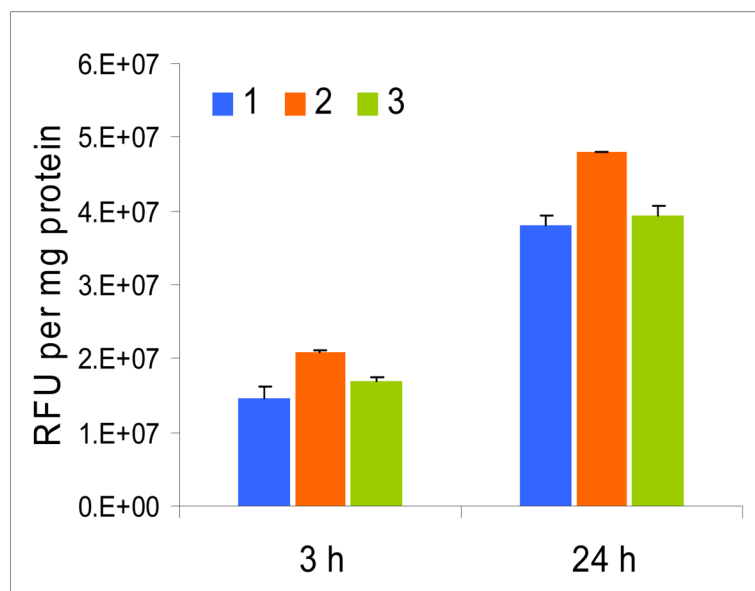


Figure 7.
In vitro uptake (RIF cells) of **1**, **2** and **3** at 3 and 24 h post-incubation.

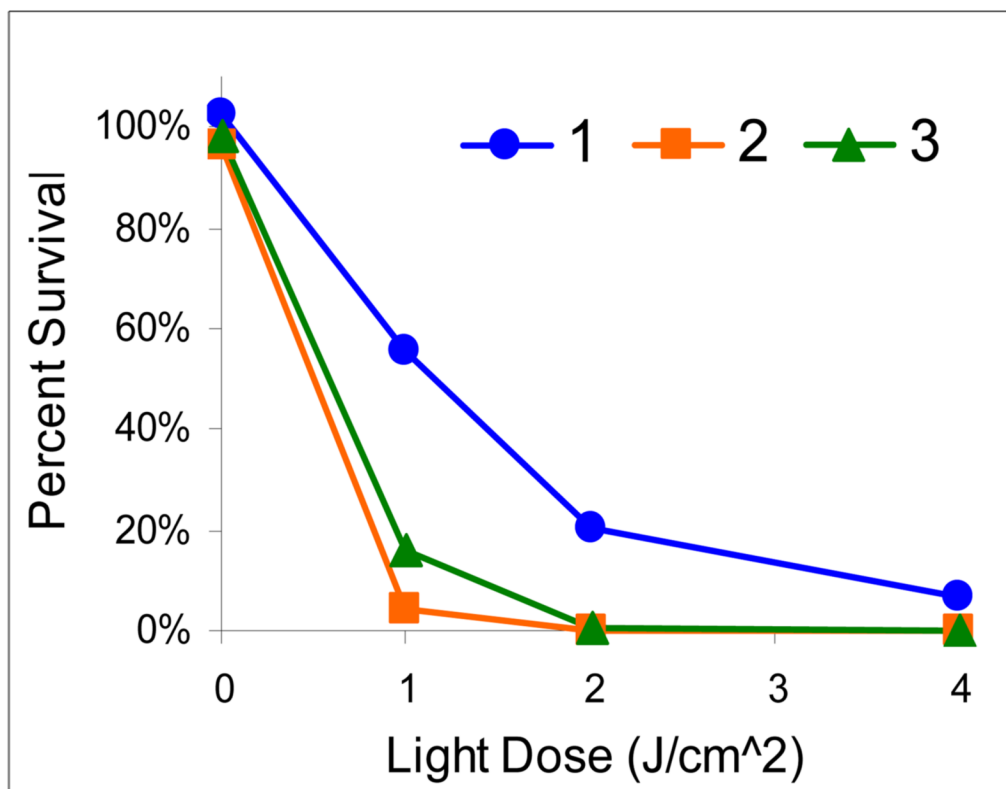


Figure 8.
In vitro phototoxicity (RIF cells) of **1**, **2** and **3** (0.25 μ M) at 24 hrs post-incubation.

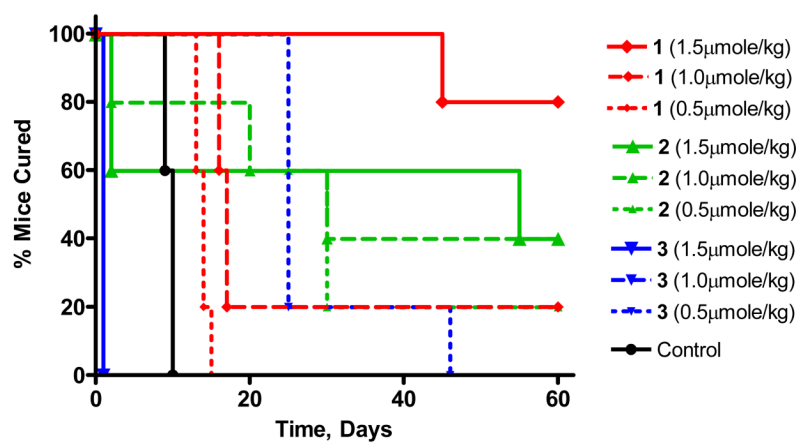
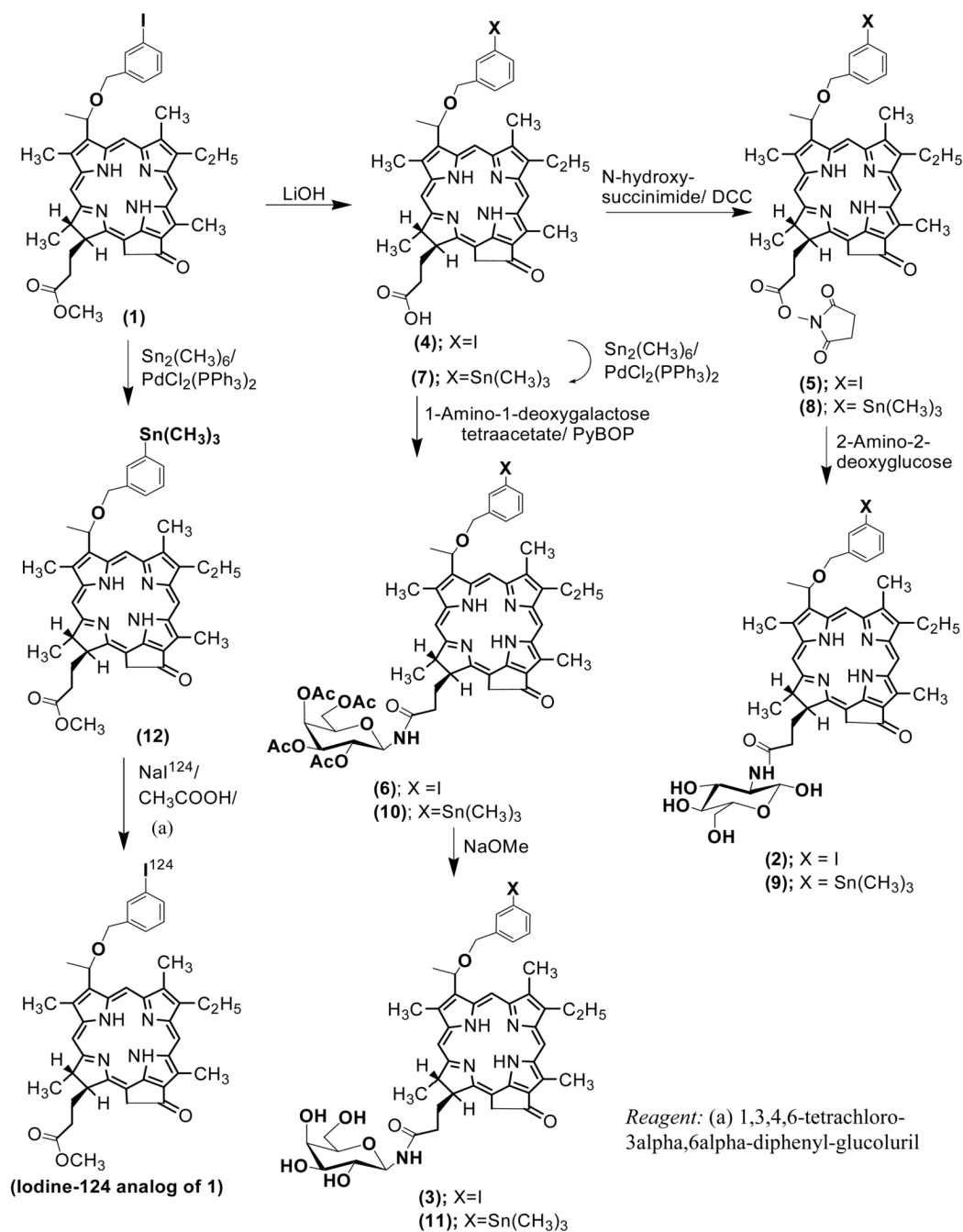


Figure 9. Kaplan Meier plot for compounds **1**, **2** and **3** at various drug doses in C3H mice bearing RIF tumor on shoulder (5 mice/group). Light dose: 135J/cm², 75 mW/cm² for 30 min at 24h post-injection.

**Scheme 1.**

Synthetic strategy for the preparation of glucose and galactose conjugates (2 and 3 respectively) from 1 and the corresponding ¹²⁴I-labeled analogs.